Journal of Solid State Chemistry 183 (2010) 1510–1520

Contents lists available at ScienceDirect

Journal of Solid State Chemistry

journal homepage: www.elsevier.com/locate/jssc

Four divalent transition metal carboxyarylphosphonate compounds: Hydrothermal synthesis, structural chemistry and generalized 2D FTIR correlation spectroscopy studies

Ran Lei [a], Xiaochuan Chai [a], Hongxin Mei [a], Hanhui Zhang [a,b,*], Yiping Chen [a], Yanqiong Sun [a]

[a] Department of Chemistry, Fuzhou University, Fuzhou, Fujian 350108, PR China
[b] State Key Laboratory of Structural Chemistry, Fujian Institute of Research on the Structure of Matter, The Chinese Academy of Sciences, Fuzhou, Fujian 350002, PR China

ARTICLE INFO

Article history:
Received 21 January 2010
Received in revised form
9 April 2010
Accepted 25 April 2010
Available online 13 May 2010

Keywords:
Hydrothermal synthesis
Carboxyarylphosphonates
Crystal structures
2D FTIR correlation analysis

ABSTRACT

Four divalent transition metal carboxyarylphosphonates, $[Ni(4,4'\text{-bipy})H_2L^1(HL^1)_2(H_2O)_2]\cdot 2H_2O$ **1**, $[Ni_2(4,4'\text{-bipy})(L^2)(OH)(H_2O)_2]\cdot 3H_2O$ **2**, $Mn(phen)_2(H_2L^1)_2$ **3** and $Mn(phen)(HL^2)$ **4** (H_3L^1=*p*-$H_2O_3PCH_2$–C_6H_4–COOH, H_3L^2=*m*-$H_2O_3PCH_2$–C_6H_4–COOH, 4,4′-bipy=4,4′-bipyridine, phen=1,10-phenanthroline) were synthesized under hydrothermal conditions. **1** features 1D linear chains built from Ni(II) ions bridging 4,4′-bipy. In **2**, neighboring Ni_4 cluster units are connected by pairs of H_3L^2 ligands to form 1D double-crankshaft chains, which are interconnected by pairs of 4,4′-bipy into 2D sheets. **3** exhibits 2D supramolecular layers via the $R_2^2(8)$ ringed hydrogen bonding units. **4** has 1D ladderlike chains, in which the 4-membered rings are cross-linked by the organic moieties of the H_3L^2 ligands. Additionally, 2D FTIR correlation analysis is applied with thermal and magnetic perturbation to clarify the structural changes of functional groups from H_3L^1 and H_3L^2 ligands in the compounds more efficiently.

1. Introduction

The synthesis of metal phosphonates has always been a research field in recent years mainly due to their potential application in the area of catalysis, proton conductivity, intercalation chemistry, magnetic studies, sorption, etc. [1–6]. It is still a difficult task to design and synthesize metal phosphonates, especially with unique zeolite-type microstructures. Additional functional groups such as aza-crown ethers, N-containing groups, hydroxyl, carboxylic groups in phosphonic acids have been used to provide varieties of coordination modes that may increase the solubility of the metal phosphonates in water, improve the crystallinity and synthesize phosphonates with varieties of structures synchronously [2,7–23]. Among them the preparation of metal phosphonates with rigid aromatic carboxylate-type ligands is still an interest, including the high-throughput synthesis of M/H_3L^1 (M=Mn, Cu, Cd, Zn, H_3L^1=*p*-$H_2O_3PCH_2C_6H_4COOH$) [24,25]. This kind of ligands may behave as a four-connected unit that can result in structures with the zeolite topology. Zhao et al. found that employing different organic amines and solvents can be effective in achieving varieties of zinc phosphonocarboxylate structures based on 4-phosphono-benzoic acid(H_2O_3P–C_6H_4–COOH, H_3pbc) [26,27].

In this article, we used two aromatic phosphonocarboxylic acids, H_3L^1 and H_3L^2 (H_3L^1=*p*-$H_2O_3PCH_2$–C_6H_4–COOH, H_3L^2=*m*-$H_2O_3PCH_2$–C_6H_4–COOH), to synthesize metal phosphonates based on the following considerations: (1) They have both phosphonate groups and carboxyl groups, which can provide multi-coordinating sites that makes it possible for structural diversity. In addition, interesting hydrogen bonds may be formed between these two groups to create supramolecular frameworks or make the crystal structures more stable. (2) The two ligands contain the flexible –CH_2– groups, which are sensitive toward metal atoms and can freely twist to meet the requirements of the coordination geometries around metal atoms [28]. (3) The two ligands hold rigid conformation that can play a role as linkers of cluster units or ringed units and thus provide probability for porous structures. Fortunately, four divalent transition metal carboxyarylphosphonates, namely, $[Ni(4,4'\text{-bipy})(H_2L^1)_2(H_2O)_2]\cdot 2H_2O$ **1**, $[Ni_2(4,4'\text{-bipy})(L^2)(OH)(H_2O)_2]\cdot 3H_2O$ **2**, $Mn(phen)_2(H_2L^1)_2$ **3** and $Mn(phen)(HL^2)$ **4**, were obtained with the two aromatic phosphonocarboxylic acids, H_3L^1 and H_3L^2 ligands, respectively, under hydrothermal conditions. In order to improve the structural diversity, especially to obtain the compounds with porous structures, the auxiliary ligands 4,4′-bipy(4,4′-bipyridine) and phen(1,10-phenanthroline) were introduced, respectively. Herein we report their syntheses and crystal structures. Additionally, we have successfully introduced the generalized 2D FTIR

* Corresponding author at: Department of Chemistry, Fuzhou University, Fuzhou, Fujian 350108, PR China. Fax: +86 591 22866340.
E-mail addresses: zhanghh1840@hotmail.com, hhzhang@fzu.edu.cn (H. Zhang).

0022-4596/$ - see front matter © 2010 Elsevier Inc. All rights reserved.
doi:10.1016/j.jssc.2010.04.037

correlation analysis proposed by Noda [29–31] to the polyoxometalates (POMs) [32,33] and coordination polymers [28,34]. The results indicate that the subtle structural changes can be clearly probed by the generalized 2D IR correlation spectroscopy. Herein, in order to clarify the structural changes of functional groups from H_3L^1 and H_3L^2 ligands in the compounds more efficiently, the generalized 2D FTIR correlation analysis is applied with thermal and magnetic perturbation, and some interesting results were obtained as well.

2. Experimental section

2.1. Materials and instrumentation

The phosphonocarboxylic acids H_3L^1 (p-$H_2O_3PCH_2$–C_6H_4–COOH) and H_3L^2 (m-$H_2O_3PCH_2$–C_6H_4–COOH) were synthesized by a classical Arbuzov reaction starting from $P(OCH_2CH_3)_3$ and $BrCH_2$–C_6H_4–COOH [35]. Other chemicals with reagent-grade quality were purchased from commercial sources and used without purification. Elemental analyses of C, H and N were performed by an Elemental Vario El III elemental analyzer. Ultraviolet–visible diffuse reflection integral spectra (UV–vis DRIS) were measured by a Perkin-Elmer Lambda 900 UV–Vis spectrometer with $BaSO_4$ as the reference sample. The infrared spectrum (4000–400 cm^{-1}) was recorded by using KBr pellets on a Perkin-Elmer 2000 FTIR spectrometer. In order to get the 2D correlation FTIR spectra, the temperature variation was controlled by a temperature controller from 50 to 120 °C at intervals of 10 °C and the magnetic intensity variation was controlled by a home-made magnetic intensity controller from 2 to 20 mT at intervals of 2 mT. By way of parenthesis introducing, the magnetic intensity was controlled by altering the voltage of Potentiostatic Apparatus that was demarcated by Gauss Meter in advance. 2D FTIR correlation spectra were obtained by treatment of the series of dynamic spectra with 2D correlation analysis of FTIR software provided by Tsinghua University.

2.2. Synthesis

2.2.1. Synthesis of $[Ni(4,4'\text{-bipy})(H_2L^1)_2(H_2O)_2]\cdot 2H_2O$ **1**

A mixture of $Ni(CH_3COO)_2\cdot 4H_2O$ (0.1244 g, 0.5 mmol), H_3L^1 (0.054 g, 0.25 mmol), 4,4′-bipy (0.096 g, 0.5 mmol) and distilled water (10 mL) was stirred for dissolution and the pH value was adjusted to 2.0 by addition of 2.0 M HCl solution before heating to 170 °C for 72 h in a Telflon-lined stainless steel autoclave (30 mL). After slow cooling to ambient temperature, light green block crystals of **1** were obtained in a yield of 60% based on Ni. Anal. Calcd. for $C_{13}H_{16}NO_7PNi_{0.5}$ (Mr=358.59): C, 43.54%; H, 4.50%; N, 3.91%. Found: C, 43.48%; H, 4.36%; N, 3.82%. IR data (KBr cm^{-1}): 3393(w), 3102(w), 2776(w), 2322(w),1670(vs), 1609(vs), 1577(m), 1417(vs), 1285(s), 1150(s), 1069(m), 820(m), 699(s), 483(m).

2.2.2. Synthesis of $[Ni_2(4,4'\text{-bipy})(L^2)(OH)(H_2O)_2]\cdot 3H_2O$ **2**

A mixture of $Ni(CH_3COO)_2\cdot 4H_2O$ (0.1244 g, 0.5 mmol), H_3L^2 (0.065 g, 0.3 mmol), 4,4′-bipy (0.096 g, 0.5 mmol) and distilled water (6.0 mL) was stirred for dissolution and the pH value was adjusted to 5.0 by addition of 2.0 M NaOH solution before heating to 170 °C for 72 h in a Telflon-lined stainless steel autoclave (13 mL). After slow cooling to ambient temperature, green block crystals of **2** were obtained in a yield of 20% based on Ni. Anal. Calcd. for $C_{18}H_{22}N_2O_{11}PNi_2$ (Mr=590.73): C, 36.60%; H, 3.75%; N, 4.74%. Found: C, 36.52%; H, 3.68%; N, 4.65%. IR data (KBr,cm^{-1}): 3568(m), 3054(w), 1610(s), 1543(vs), 1413(s), 1385(s),1197(s), 1027(s), 965(vs), 811(s), 764(s), 509(m).

2.2.3. Synthesis of $Mn(phen)_2(H_2L^1)_2$ **3**

A mixture of $MnCl_2\cdot 4H_2O$ (0.1980 g, 1.0 mmol), H_3L^1 (0.108 g, 0.50 mmol), phen (0.0496 g, 0.25 mmol) and distilled water (5.0 mL) was stirred for dissolution and the pH value was adjusted

Table 1
Crystallographic data for compounds **1**, **2**, **3** and **4**.

Compound	**1**	**2**	**3**	**4**
Empirical formula	$C_{13}H_{16}NO_7PNi_{0.5}$	$C_{18}H_{22}N_2O_{11}PNi_2$	$C_{20}H_{16}N_2O_5PMn_{0.5}$	$C_{20}H_{15}N_2O_5PMn$
Formula weight	358.59	590.77	422.79	449.25
Crystal system	Orthorhombic	Triclinic	Monoclinic	Triclinic
Space group	*Pccn*	*P*−1	*C*2/*c*	*P*−1
a (Å)	9.0157(18)	8.4836(17)	9.995(2)	9.4598(19)
b (Å)	14.080(3)	11.512(2)	21.610(4)	10.258(2)
c (Å)	22.688(5)	12.793(3)	18.456(4)	10.769(2)
α (deg.)	90.00	112.97(3)	90.00	75.03(3)
β (deg.)	90.00	96.36(3)	102.10(3)	69.49(3)
γ (deg.)	90.00	94.30(3)	90.00	83.95(3)
V (Å^3)	2880.0(10)	1133.8(4)	3897.7(13)	945.4(3)
Z	8	2	8	2
D_{calcd} (g/cm^3)	1.654	1.730	1.441	1.578
F(0 0 0)	1488	606	1740	458
λ(Mo*K*α) (Å)	0.71073	0.71073	0.71073	0.71073
Limiting indices	$-11\le h\le 11$; $-18\le k\le 17$; $-25\le l\le 29$	$-11\le h\le 11$; $-14\le k\le 12$; $-16\le l\le 16$	$-12\le h\le 12$; $-28\le k\le 19$; $-23\le l\le 23$	$-12\le h\le 12$; $-13\le k\le 9$; $-13\le l\le 13$
Goodness-of-fit on F^2	1.017	1.022	1.014	1.031
μ (mm^{-1})	0.862	1.794	0.485	0.819
Total data collect.	21750	9550	16149	7863
Unique/obs.data ($I>2\sigma(I)$)	3265/3315	4982/4724	4382/4249	4157/4003
R_1[a],wR_2[b] [$I>2\sigma(I)$]	0.0699, 0.2609	0.0457, 0.1409	0.0415, 0.1192	0.0353, 0.0864
R_1,wR_2 (all data)	0.0711, 0.2629	0.0484, 0.1437	0.0432, 0.1207	0.0373, 0.0899
Δe min/max (eÅ^{-3})	−1.203/0.451	−0.609/1.125	−0.333/0.250	−0.303/0.307

[a] $R_1=\sum||F_0|-|F_c||/\sum|F_0|$.
[b] $wR_2=\{\sum[w(F_0^2-F_c^2)^2]/\sum[w(F_0^2)^2]\}^{1/2}$.

Table 2
Selected bond lengths (Å) and angles (deg.) for $[Ni(4,4'\text{-bipy})(H_2L^1)_2(H_2O)_2]\cdot 2H_2O$ **1**[a].

Ni(1)–O(5)#1	2.076(3)	Ni(1)–O(5)	2.076(3)
Ni(1)–OW1#1	2.104(4)	Ni(1)–OW1	2.104(4)
Ni(1)–N(1)#2	2.112(5)	Ni(1)–N(2)	2.117(6)
P(1)–O(5)	1.495(4)	P(1)–O(4)	1.514(3)
P(1)–O(3)	1.577(3)	P(1)–C(8)	1.813(5)
O(1)–C(1)	1.202(7)	O(2)–C(1)	1.291(7)
O(5)–Ni(1)–O(5)#1	179.84(16)	O(5)–Ni(1)–OW1#1	91.44(14)
O(5)#1–Ni(1)–OW1#1	88.55(14)	O(5)–Ni(1)–OW1	88.55(14)
O(5)#1–Ni(1)–OW1	91.44(14)	OW1#1–Ni(1)–OW1	178.34(18)
O(5)–Ni(1)–N(1)#2	89.92(8)	O(5)#1–Ni(1)–N(1)#2	89.92(8)
OW1#1–Ni(1)–N(1)#2	89.17(9)	OW1–Ni(1)–N(1)#2	89.17(9)
O(5)–Ni(1)–N(2)	90.08(8)	O(5)#1–Ni(1)–N(2)	90.08(8)
OW1#1–Ni(1)–N(2)	90.83(9)	OW1–Ni(1)–N(2)	90.83(9)
N(1)#2–Ni(1)–N(2)	180.0		

[a] #1 $-x+1/2, -y+1/2, z$; #2 $-x+1/2, y, z+1/2$.

to 2.0 by addition of 2.0 M NaOH solution before heating to 160 °C for 72 h in a Telflon-lined stainless steel autoclave (13 mL). After slow cooling to ambient temperature, light yellow block crystals of **3** were obtained in a yield of 80% based on Mn. Anal. Calcd. for $C_{20}H_{16}N_2O_5PMn_{0.5}$ (Mr=422.79): C, 56.82%; H, 3.82%; N, 6.63%. Found: C, 56.74%; H, 3.76%; N, 6.57%. IR data (KBr cm^{-1}): 3406(vw), 3042(w), 2784(w), 2431(w), 1689(vs), 1608(vs), 1516(vs), 1425(vs), 1283(s), 1196(s), 1017(s), 847(vs), 699(s), 474(s).

2.2.4. Synthesis of Mn(phen)(HL^2) **4**

A mixture of $MnCl_2\cdot 4H_2O$ (0.1980 g, 1.0 mmol), H_3L^2 (0.0648 g, 0.30 mmol), phen (0.0991 g, 0.50 mmol) and distilled water (10.0 mL) was stirred for dissolution and the pH was adjusted to 3.5 by addition of 2.0 M NaOH solution. After stirring for several minutes, 0.06 g NaF was added before heating to 160 °C for 72 h in a Telflon-lined stainless steel autoclave (30 mL). After slow cooling to ambient temperature, light yellow block crystals of **4** were obtained in a yield of 80% based on Mn. Anal. Calcd. for $C_{20}H_{15}N_2O_5PMn$ (Mr=449.25): C, 53.47%; H, 3.37%; N, 6.24%. Found: C, 53.35%; H, 3.25%; N, 6.11%. IR data (KBr cm^{-1}): 3434(vw), 3058(w), 2789(vw), 2344(vw), 1593(s), 1550(vs), 1393(vs), 1180(s), 1076(s), 937(s), 846(vs), 729(vs), 522(vs), 431(m).

2.3. X-ray crystallography

The single-crystal X-ray diffraction data were collected on a Rigaku Saturn 724 CCD diffraction by a graphite-monochromatized Mo$K\alpha$ radiation (λ=0.71073 Å) using an ω scan mode in the range of $3.05<\theta<27.54^\circ$ at 293(2) K. The data sets were corrected for absorption by a multi-scan technique. The structures were solved by direct methods and refined by full-matrix least-squares on F^2 with SHELXTL-97 [36,37]. All non-hydrogen atoms were refined with anisotropic thermal parameters. All hydrogen atoms were located at the geometrically calculated positions and refined with isotropic thermal parameters. Hydrogen atoms for water molecules in compounds **1** and **2** were not included in the refinements. For compound **1**, OW2A and OW2B (O–O distance: 1.544(17) Å) are considered to be two orientations of a disordered water molecule. OW2A is refined with 40% occupancy and OW2B with 60% occupancy. The crystallographic data for four compounds are summarized in Table 1. Selected bond distances and angels are given in Tables 2–5. The corresponding parameters for O–H$\cdots$O hydrogen bonds and C–H$\cdots\pi$ interactions are listed in Table 6. The corresponding parameters for π–π stacking interactions between selected rings are listed in Table 7.

Table 3
Selected bond lengths (Å) and angles (deg.) for $[Ni_2(4,4'\text{-bipy})(L^2)(OH)(H_2O)_2]\cdot 3H_2O$ **2**[a].

Ni(1)–O(6)#1	2.034(2)	Ni(1)–O(2)	2.051(2)
Ni(1)–O(6)	2.066(2)	Ni(1)–N(2)#2	2.093(3)
Ni(1)–O(4)#3	2.097(2)	Ni(1)–O(7)	2.105(2)
Ni(2)–O(6)	1.989(2)	Ni(2)–O(1)	2.049(2)
Ni(2)–O(8)	2.062(3)	Ni(2)–N(1)	2.067(3)
Ni(2)–O(7)	2.136(2)	Ni(2)–O(4)#4	2.193(2)
P(1)–O(3)	1.526(3)	P(1)–O(5)	1.533(3)
P(1)–O(4)	1.547(2)	P(1)–C(8)	1.801(3)
O(1)–C(1)	1.262(4)	O(2)–C(1)	1.266(4)
O(4)–Ni(1)#3	2.097(2)	O(4)–Ni(2)#5	2.193(2)
O(6)–Ni(1)#1	2.034(2)		
O(6)#1–Ni(1)–O(2)	169.81(10)	O(6)#1–Ni(1)–O(6)	79.91(10)
O(2)–Ni(1)–O(6)	91.28(10)	O(6)#1–Ni(1)–N(2)#2	98.57(11)
O(2)–Ni(1)–N(2)#2	89.48(11)	O(6)–Ni(1)–N(2)#2	172.28(10)
O(6)#1–Ni(1)–O(4)#3	82.27(10)	O(2)–Ni(1)–O(4)#3	103.81(10)
O(6)–Ni(1)–O(4)#3	95.32(10)	N(2)#2–Ni(1)–O(4)#3	91.96(11)
O(6)#1–Ni(1)–O(7)	87.28(10)	O(2)–Ni(1)–O(7)	86.56(10)
O(6)–Ni(1)–O(7)	83.00(10)	N(2)#2–Ni(1)–O(7)	89.38(11)
O(4)#3–Ni(1)–O(7)	169.55(9)	O(6)–Ni(2)–O(1)	92.69(11)
O(6)–Ni(2)–O(8)	173.37(10)	O(1)–Ni(2)–O(8)	90.90(11)
O(6)–Ni(2)–N(1)	96.23(12)	O(1)–Ni(2)–N(1)	99.03(11)
O(8)–Ni(2)–N(1)	88.71(12)	O(6)–Ni(2)–O(7)	84.07(10)
O(1)–Ni(2)–O(7)	86.75(10)	O(8)–Ni(2)–O(7)	90.57(10)
N(1)–Ni(2)–O(7)	174.18(11)	O(6)–Ni(2)–O(4)#4	80.90(9)
O(1)–Ni(2)–O(4)#4	168.33(10)	O(8)–Ni(2)–O(4)#4	94.59(10)
N(1)–Ni(2)–O(4)#4	91.39(11)	O(7)–Ni(2)–O(4)#4	82.92(9)

[a] #1 $-x+1, -y+1, -z+1$; #2 $x, y+1, z+1$; #3 $-x+1, -y+2, -z+1$; #4 $x, y-1, z$.

Table 4
Selected bond lengths (Å) and angles (deg.) for $Mn(phen)_2(H_2L^1)_2$ **3**[a].

Mn(1)–O(2)	2.0605(14)	Mn(1)–O(2)#1	2.0605(14)
Mn(1)–N(1)#1	2.2834	Mn(1)–N(1)	2.2834
Mn(1)–N(2)	2.3192	Mn(1)–N(2)#1	2.3192
P(1)–O(2)	1.4847(14)	P(1)–O(1)	1.5118(13)
P(1)–O(3)	1.5685(10)	P(1)–C(1)	1.8062
O(4)–C(8)	1.310(2)	O(5)–C(8)	1.196(2)
O(2)–Mn(1)–O(2)#1	94.83(9)	O(2)–Mn(1)–N(1)#1	105.13(5)
O(2)#1–Mn(1)–N(1)#1	90.82(5)	O(2)–Mn(1)–N(1)	90.82(5)
O(2)#1–Mn(1)–N(1)	105.13(5)	N(1)#1–Mn(1)–N(1)	156.5
O(2)–Mn(1)–N(2)	162.52(4)	O(2)#1–Mn(1)–N(2)	92.38(5)
N(1)#1–Mn(1)–N(2)	90.6	N(1)–Mn(1)–N(2)	71.9
O(2)–Mn(1)–N(2)#1	92.38(5)	O(2)#1–Mn(1)–N(2)#1	162.52(4)
N(1)#1–Mn(1)–N(2)#1	71.9	N(1)–Mn(1)–N(2)#1	90.6
N(2)–Mn(1)–N(2)#1	85.3		

[a] #1 $-x+1, y, -z+1/2$.

3. Results and discussion

3.1. Structural description

$[Ni(4,4'\text{-bipy})(H_2L^1)_2(H_2O)_2]\cdot 2H_2O$ **1**. As shown in Fig. 1, the Ni(II) ion in the structure of compound **1** is six-coordinated by two phosphonate oxygen atoms (O5, O5B) from two H_3L^1 ligands, two nitrogen atoms (N2, N1A) from two 4,4′-bipy ligands, and two oxygen atoms (OW1, OW1C) from two aqua ligands. The Ni–O distances are 2.076(3) and 2.104(4) Å, respectively, and the Ni–N distances are 2.112(5) and 2.117(6) Å in turn. These distances are comparable to those in other Ni(II) phosphonates [38]. Only one oxygen atom (O5) from H_3L^1 ligand which adopts monodentate coordination mode is coordinated. Based on C–O, P–O distances and charge balance, O2 and O3 are 1H-protonated. The structure of compound **1** has a type of $R_2^2(8)$ ringed hydrogen bonding units which are composed of two phosphonate groups and two O3–H30$\cdots$O4 (symmetry code: $-x+1, -y+1, -z$) hydrogen bonds

(Fig. 2) [39]. The Ni(II) ions are bridged by 4,4′-bipy rings to generate 1D chains along *c*-axis. Along the same chain, the aromatic rings of the H_3L^1 ligands which coordinate with the Ni(II) ions stretch in the same direction. Such neighboring chains are further connected by the $R_2^2(8)$ ringed hydrogen bonding units and the linking between the $R_2^2(8)$ ringed hydrogen bonding units and another H_3L^1 ligand via strong O2–H20···O4 (symmetry code: $x-1/2$, $-y+1$, $-z+1/2$) hydrogen bonds into a 3D supramolecular framework (Fig. 3), which is consolidated by the OW1–HW1B···O4 (symmetry code: $-x+1/2$, $-y+1/2$, z) and OW1–HW1A···OW2A/OW2B hydrogen bonds (Table 6). The lattice water molecules which form hydrogen bonds with aqua

Table 5
Selected bond lengths (Å) and angles (deg.) for Mn(phen)(HL^2) **4**[a].

Mn(1)–O(4)#1	2.0393(19)	Mn(1)–O(3)#2	2.0463(15)
Mn(1)–O(2)	2.0469(16)	Mn(1)–N(2)	2.2756(18)
Mn(1)–N(1)	2.2964(18)	P(1)–O(2)	1.4967(15)
P(1)–O(3)	1.4994(15)	P(1)–O(1)	1.5629(18)
P(1)–C(1)	1.801(2)	O(3)–Mn(1)#2	2.0463(15)
O(4)–Mn(1)#1	2.0393(19)	O(4)–C(7)	1.248(3)
O(5)–C(7)	1.234(3)		
O(4)#1–Mn(1)–O(3)#2	107.36(7)	O(4)#1–Mn(1)–O(2)	106.87(9)
O(3)#2–Mn(1)–O(2)	101.78(7)	O(4)#1–Mn(1)–N(2)	93.79(7)
O(3)#2–Mn(1)–N(2)	153.20(7)	O(2)–Mn(1)–N(2)	87.09(7)
O(4)#1–Mn(1)–N(1)	101.46(8)	O(3)#2–Mn(1)–N(1)	87.28(6)
O(2)–Mn(1)–N(1)	145.85(7)	N(2)–Mn(1)–N(1)	72.21(6)

[a] #1 $-x+1$, $-y+1$, $-z$; #2 $-x+1$, $-y$, $-z$.

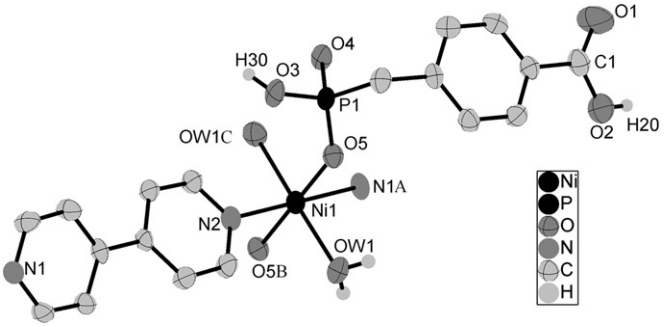

Fig. 1. ORTEP representation of the selected unit of compound **1** (50% thermal ellipsoids probability); the lattice water molecule and the H atoms attached to C atoms are omitted for clarity; symmetry codes: A, $-x+1/2, -y+1/2, z$; B, $-x+1/2, y, z+1/2$; C, $-x+1/2, y, z-1/2$; D, $-x-1/2, -y+1/2, z$.

Table 6
Parameters for O–H···O hydrogen bonds and C–H···π interactions.

Compounds	D–H···A	d(D–H) (Å)	d(H·A) (Å)	d(D……A) (Å)	< DHA (deg.)
1	OW1–HW1A···OW2B	0.843	1.893	2.734	175.00
	OW1–HW1A···OW2A	0.843	2.150	2.785	131.95
	OW1–HW1B···O4#1	0.844	2.204	2.954	147.94
	O2–H20···O4#2	0.848	1.789	2.633	173.44
	O3–H30···O4#3	0.847	1.768	2.612	172.98
2	O6–H6O···O5#1	0.848	2.304	2.976	136.43
	O7–H7OA···O5#2	0.841	1.940	2.729	155.79
	O7–H7OA···O6#3	0.841	2.437	2.857	111.75
	O7–H7OB···O3#4	0.852	1.705	2.542	166.46
	O8–H8OA···O3#2	0.871	1.816	2.676	168.48
	O8–H8OB···O5#4	0.853	1.903	2.722	160.34
	C8–H8B···Cg(21)#5	—	2.68	3.6579	168
3	O3–H21···O1#1	0.784	1.832	2.615	176.73
	O4–H22···O1#2	0.929	1.668	2.573	163.59
4	O1–H1···O5#1	0.840	1.763	2.541	153.32
	C3–H3···Cg(2)#2	—	2.78	3.6522	154
	C20–H20···Cg(4)#3	—	2.89	3.5998	132

Compound **1**: #1 $-x+1/2$, $-y+1/2$, z; #2 $x-1/2$, $-y+1$, $-z+1/2$; #3 $-x+1$, $-y+1$, $-z$.
Compound **2**: #1 $-x+1$, $-y+2$, $-z+1$; #2 x, $y-1$, z; #3 $-x+1$, $-y+1$, $-z+1$; #4 $-x$, $-y+2$, $-z+1$; #5 $-x$, $-y$, $1-z$. Cg(21): C(2), C(3), C(4), C(5), C(6), C(7).
Compound **3**: #1 $-x+2$, y, $-z+1/2$; #2 x, $-y+1$, $z+1/2$.
Compound **4**: #1 x, $y-1$, z; #2 $-1+x$, y, z; #3 x, y, z. Cg(2): N(1), C(9), C(10), C(11), C(12), C(13) ;Cg(4): C(2), C(3), C(4), C(5), C(6), C(8).

Table 7
Parameters for π–π stacking interactions between selected rings.

Compounds	Two rings	Centroid-to-centroid distance (Å)	Dihedral angels (deg.)	Perpendicular distance of Cg(I) on ring J (Å)	Perpendicular distance of Cg(J) on ring I (Å)
2	Cg(1) > Cg(1)#1	3.0574(7)	0.00	2.024	2.024
	Cg(19) > Cg(20)#2	3.6295	7.20	3.405	3.513
3	Cg(3) > Cg(6)#1	3.8033	1.27	3.555	3.544
4	Cg(1) > Cg(2) #1	3.6765	0.64	3.415	3.409
	Cg(1) > Cg(5)#1	3.7127	0.22	3.412	3.410
	Cg(2) > Cg(3)#1	3.7169	0.63	3.411	3.427
	Cg(2) > Cg(5)#1	3.6382	0.44	3.416	3.407

Compound **2**: #1 $1-x$, $1-y$, $1-z$; #2 $1-x$, $-y$, $-z$. Cg(1): Ni(1), O(4), Ni(2), O(6); Cg(19): N(1), C(9), C(10), C(11), C(12), C(13); Cg(20): N(2), C(16), C(15), C(14), C(18), C(17).
Compound **3**: #1 $3/2-x, 1/2-y, 1-z$. Cg(3) : N(1), C(14), C(18), C(17), C(16), C(15); Cg(6): C(12), C(13), C(14), C(18), C(19), C(20).
Compound **4**: #1 $1-x$, $-y$, $1-z$. Cg(1) : Mn(1), N(1), C(13), C(14), N(2); Cg(2): N(1), C(9), C(10), C(11), C(12), C(13); Cg(3): N(2), C(14), C(15), C(18), C(19), C(20); Cg(5): C(12), C(13), C(14), C(15), C(16), C(17).

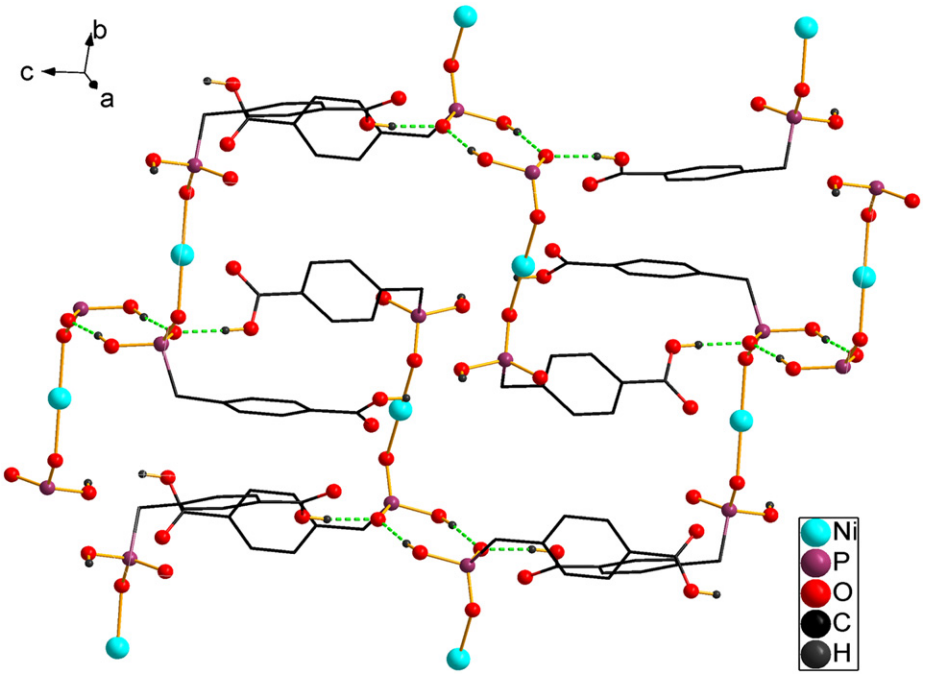

Fig. 2. A view of the connectivities via the $R_2^2(8)$ ringed hydrogen bonding units and O2–H20 · · · O4 hydrogen bonds in compound **1**; the 4,4′-bipy ligands, the lattice water molecules and the H atoms attached to C atoms are omitted for clarity; the hydrogen bonds are drawn in dashed lines.

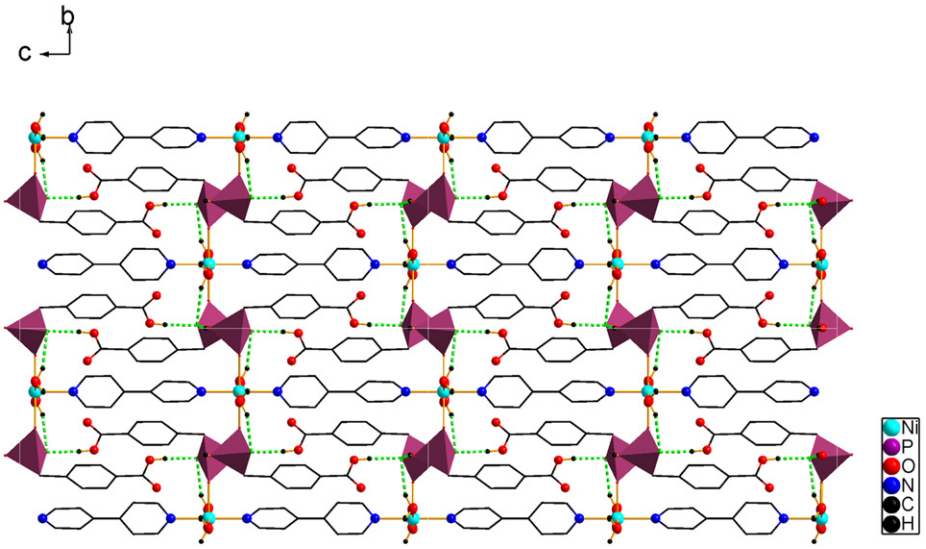

Fig. 3. A view of the 3D framework of compound **1** down *a*-axis; the lattice water molecules and the H atoms attached to C atoms are omitted for clarity; the CPO_3 groups are represented in polyhedron; the hydrogen bonds are drawn in dashed lines.

ligands are located between the neighboring 1D chains and are omitted for clarity.

$[Ni_2(4,4'\text{-bipy})(L^2)(OH)(H_2O)_2]\cdot 3H_2O$ **2**. As shown in Fig. 4, the asymmetric unit of compound **2** consists of two Ni(II) ions, one $(L^2)^{3-}$ anion, one 4,4′-bipy ligand, three aqua ligands and three lattice water molecules which are omitted for clarity. Ni1 is six-coordinated by one carboxylic oxygen atom (O2) from one H_3L^2 ligand, one phosphonate oxygen atom (O4C) from another H_3L^2 ligand, one nitrogen atom (N2D) from one 4,4′-bipy ligand and three aqua ligands (O6, O6B, O7). The Ni1–N distance is 2.093(3) Å and the Ni1–O distances are in the range 2.034(2)–2.105(2) Å. Ni2 is also six-coordinated by one carboxylic oxygen atom (O1) from one H_3L^2 ligand, one phosphonate oxygen atom (O4A) from another H_3L^2 ligand, one nitrogen atom (N1) from one 4,4′bipy ligand and three aqua ligands (O6, O7, O8). The Ni2–N distance is 2.067(3) Å and the Ni2–O distances are in the range 1.989(2)–2.193(2) Å. All these distances are comparable to those reported in other similar Ni(II) compounds [40,41]. The H_3L^2 ligand adopts tetradentate coordination mode. The carboxylate group bidentately bridges with two unique Ni(II) ions (Ni1, Ni2). The CPO_3 group bridges with two other unique Ni(II) ions, of which O4 is the bidentate metal linker and the other two phosphonate oxygen atoms are non-coordinated. Based on C–O, P–O distances, the H_3L^2 ligand is completely deprotonated and exhibits 3—in charge. The three aqua ligands adopt mono-, bi- and tri-dentate coordination mode, respectively.

There exist Ni_4 cluster units which are composed via coordinated phosphonate oxygen atoms, carboxylic oxygen atoms and three types of aqua ligands adopting different coordination modes in the structure of compound **2** (Fig. 5a). This type of Ni_4 cluster units are comparable to those reported in other similar compounds [42,43]. The Ni–Ni distances in a Ni_4 cluster unit range from 3.0420(16) to 5.3247(21)Å. To keep charge balance, one aqua ligand tridentate is assigned as $[OH]^-$. There are four types of hydrogen bonds in one Ni_4 cluster unit (Table 6). Additionally, there exists π–π stacking interaction between two metal chelated 4-membered rings in one Ni_4 cluster unit (Table 7). These hydrogen bonds and π–π stacking interactions make the Ni_4 clusters more stable. Neighboring Ni_4 cluster units are connected by pairs of H_3L^2 ligands (between which there are weak C–H···π interactions, Table 6), in which the directions of aromatic rings are different, to give rise to 1D double-crankshaft chains along *b*-axis. Such 1D chains are interconnected by pairs of 4,4′-bipy ligands (between which there exist π–π stacking interactions, Table 7) into 2D sheets on *bc* plane, displaying windows with approximately 11.5 × 11.2 Å (Fig. 5b), which are further linked via O8–H8OB···O5 (symmetry code: $-x$, $-y+2$, $-z+1$) and O7–H7OB···O3 (symmetry code: $-x$, $-y+2$, $-z+1$) hydrogen bonds into a 3D supramolecular architecture (Fig. 6). Part of the lattice water molecules are distributed on both sides of the pyridyl rings of 4,4′-bipy ligands and the others are located at the tunnels between sheets and sheets.

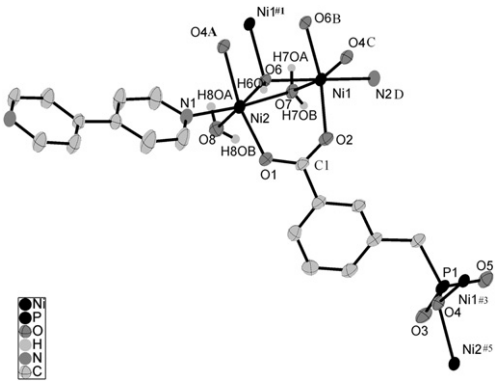

Fig. 4. ORTEP representation of the selected unit of compound **2** (50% thermal ellipsoids probability); the lattice water molecules and the H atoms attached to C atoms are omitted for clarity; symmetry codes: A, $-x+1$, $-y+1$, $-z+1$; B, x, $y+1$, $z+1$; C, $-x+1$, $-y+2$, $-z+1$; D, x, $y-1$, z; E, x, $y+1$, z; F, x, $y-1$, $z-1$.

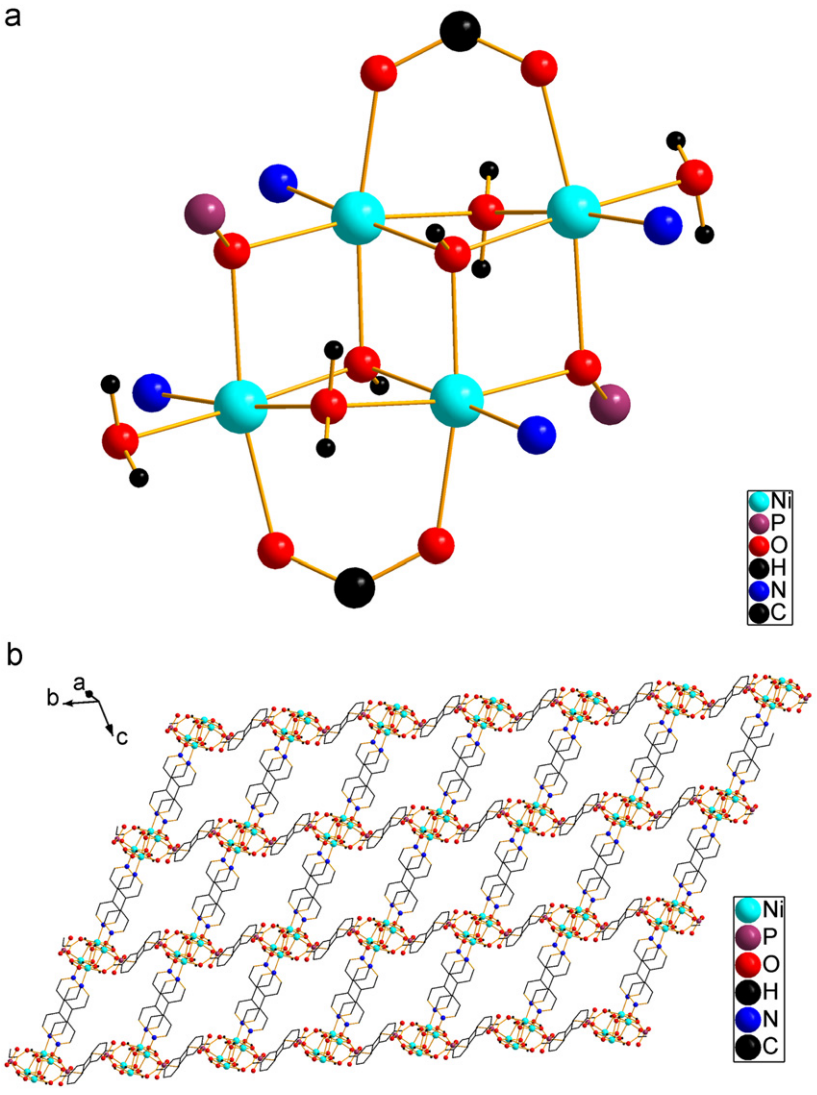

Fig. 5. (a) A schematic view of the Ni_4 cluster unit in compound **2**. (b) Diagram of the 2D sheet of compound **2**; the lattice water molecules and the H atoms attached to C atoms are omitted for clarity.

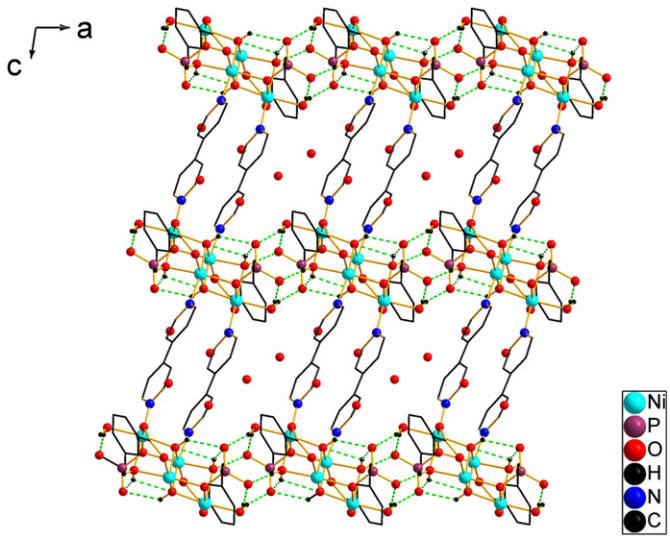

Fig. 6. A view of the crystal structure of compound **2** down *b*-axis; the H atoms attached to C atoms are omitted for clarity; the hydrogen bonds are drawn in dashed lines.

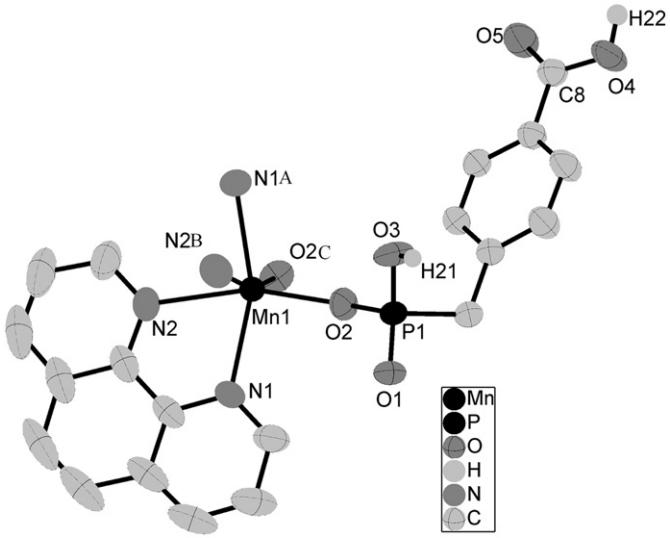

Fig. 7. ORTEP representation of the selected unit of compound **3** (50% thermal ellipsoids probability); the H atoms attached to C atoms are omitted for clarity; symmetry code: $-x+1, y, -z+1/2$.

$Mn(phen)_2(H_2L^1)_2$ **3.** As shown in Fig. 7, the Mn(II) ion is six-coordinated by two phosphonate atoms (O2, O2C) from two H_3L^1 ligands and four nitrogen atoms (N1, N2, N1A, N2B) from two bidentate chelating phen ligands. Two of the Mn–N distances are 2.2834 Å and the other two of those are 2.3192 Å. The Mn–O distances are both 2.0605(14) Å, which are comparable to those in other similar Mn(II) compounds [44]. Only one oxygen atom (O2) from H_3L^1 ligand which adopts monodentate coordination mode is coordinated. Based on C–O, P–O distances and charge balance, O3, O4 are 1H-protonated. The structure of compound **3** has a type of $R_2^2(8)$ ringed hydrogen bonding units which are composed of two phosphonate groups and O3–H21···O1 (symmetry code: $-x+2, y, -z+1/2$) hydrogen bonds as well as that in compound **1** (Fig. 8). The Mn(II) ions bridging H_3L^1 ligands are interconnected via the $R_2^2(8)$ ringed hydrogen bonding units and strong O4–

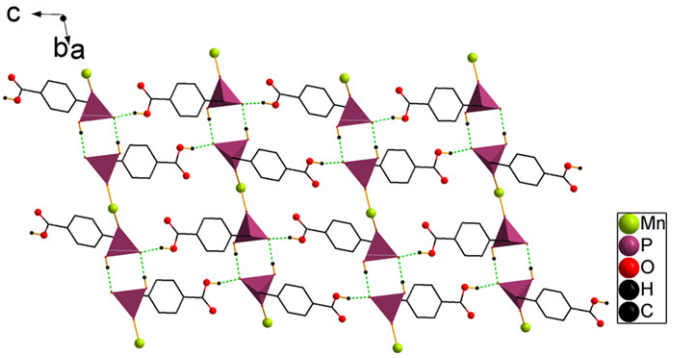

Fig. 8. A view of the connectivities via the $R_2^2(8)$ ringed hydrogen bonding units and O4–H22···O1 hydrogen bonds in compound **3**; the phen ligands and the H atoms attached to C atoms are omitted for clarity; the CPO_3 groups are represented in polyhedron; the hydrogen bonds are drawn in dashed lines.

H22···O1(symmetry code: $x, -y+1, z+1/2$) hydrogen bonds into 2D supramolecular layers on *ac* plane, which are further linked via π–π stacking interactions between phen ligands (Table 7) to form a 3D supramolecular framework (Fig. 9).

$Mn(phen)(HL^2)$ **4.** As shown in Fig. 10, the asymmetric unit of compound **4** contains one unique Mn(II) ion, one H_3L^2 ligand and one phen ligand. The Mn(II) ion is five-coordinated by two phosphonate oxygen atoms (O2, O3A) from two H_3L^2 ligands, one carboxylic oxygen atom (O4B) from another H_3L^2 ligand and two nitrogen atoms (N1, N2) from one bidentate chelating phen ligand. The Mn–O distances range from 2.0393(19) to 2.0469(16) Å, which are comparable to the similar Mn(II) compounds [45]. The Mn–N distances are 2.2756(18) and 2.2964(18) Å, respectively. The coordination geometry around the Mn(II) ion could be described as a distorted square pyramid. The H_3L^2 ligand acts as a tridentate ligand, which bridges with three Mn(II) ions. Two phosphonate oxygen atoms (O2, O3) and one carboxylic oxygen atom (O4) are metal monodentate linkers, with the two other oxygen atoms of the H_3L^2 ligand free coordinated. Based on C–O, P–O distances and charge balance, O1 is 1H-protonated. A type of 4-membered rings composed of two Mn(II) ions and two CPO_3 groups are formed in the structure of compound **4**. These 4-membered rings are cross-linked by the organic moieties of the H_3L^2 ligands to give rise to 1D ladderlike chains along *b*-axis (Fig. 11). Strong O1–H1···O5 (symmetry code: $x, y-1, z$) hydrogen bonds exist in the structure which make the 1D chains more stable. Neighboring chains are interlinked via π–π stacking interactions between phen ligands (Table 7) to form 2D supramolecular layers on *bc* plane, among which there also exist weak C–H···π interactions (Table 6), making the layers stack together (Fig. 12).

3.2. Synthetic conditions

The synthetic conditions are important for crystal growth. For compound **1** and **3**, under the condition of pH=2.0, one phosphonate oxygen atom from the H_3L^1 ligand was deprotonated. In addition, the H_3L^1 ligand adopts the same coordination mode in the two compounds, which both have the same type of $R_2^2(8)$ ringed hydrogen bonding units. Under the condition of pH=3.5 (adding NaF improves the pH value faintly), one phosphonate oxygen atom and one carboxylic oxygen atom from the H_3L^2 ligand were deprotonated, which led to the formation of compound **4**. As to compound **2**, under the condition of pH=5.0, all protons are removed. It could be concluded that pH value in synthesis has strong effect on the structures of metal

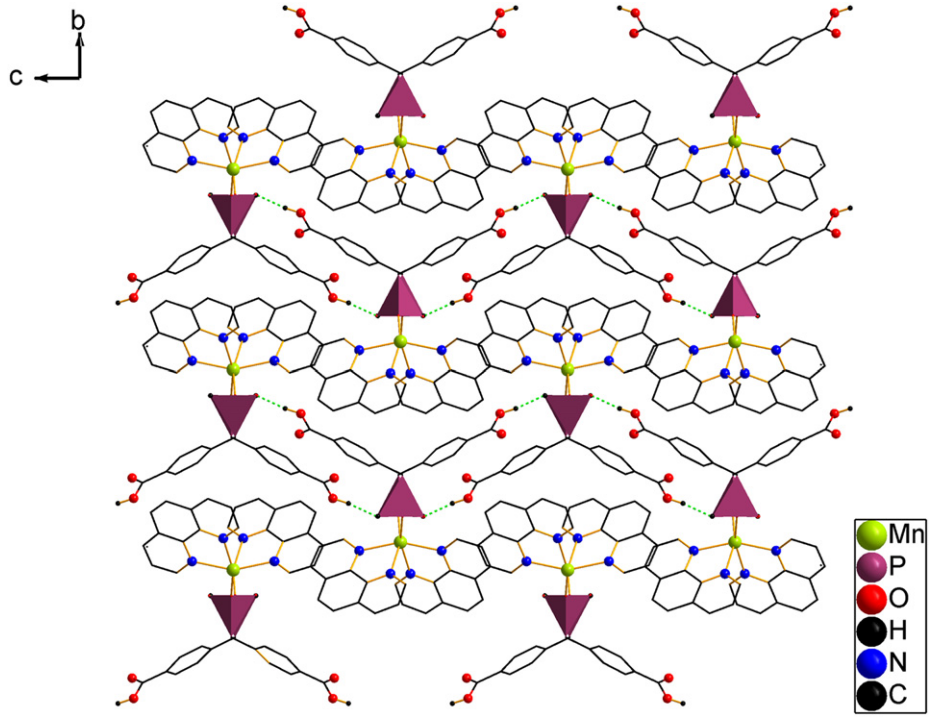

Fig. 9. A view of the crystal structure of compound **3** down *a*-axis; the CPO_3 groups are represented in polyhedron; the H atoms attached to C atoms are omitted for clarity; the hydrogen bonds are drawn in dashed lines.

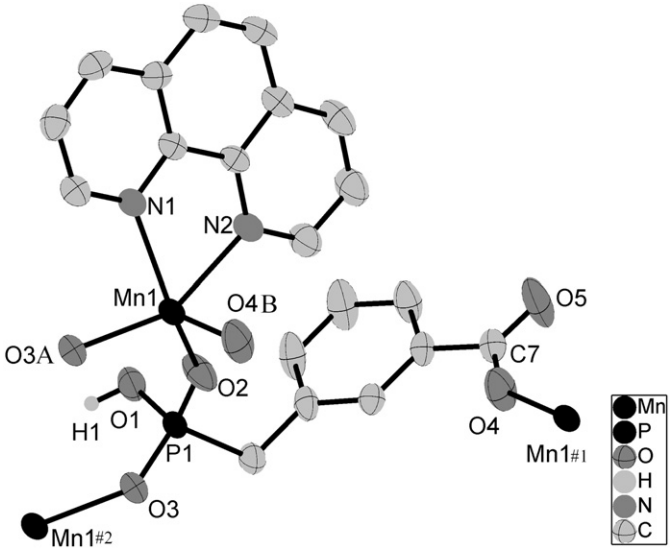

Fig. 10. ORTEP representation of the selected unit of compound **4** (50% thermal ellipsoids probability); the H atoms attached to C atoms are omitted for clarity; symmetry codes: A, $-x+1,-y+1,-z$; B, $-x+1,-y,-z$.

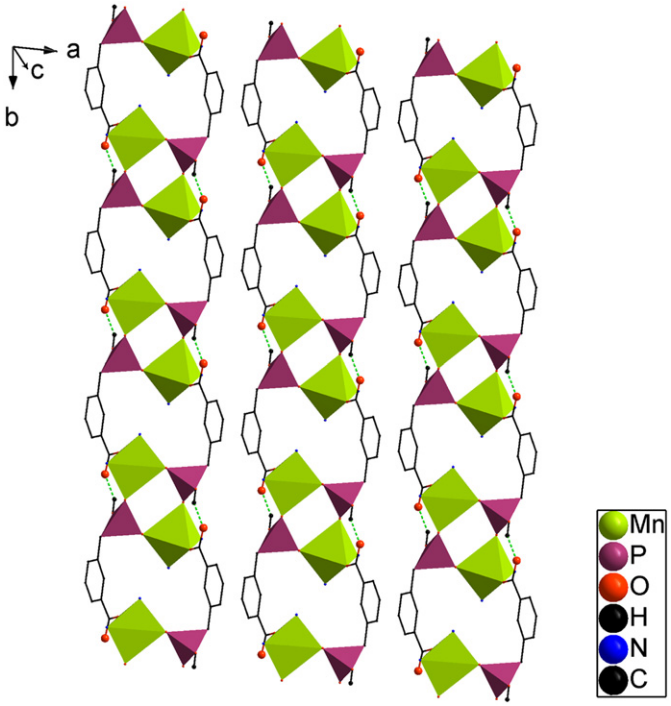

Fig. 11. Diagram of 1D ladderlike chains in compound **4** along *b*-axis; the phen ligands and the H atoms attached to C atoms are omitted for clarity; the hydrogen bonds are drawn in dashed lines; polyhedron color codes: Mn(yellow-green polyhedron), P(purple polyhedron). (For interpretation of the references to color in this figure legend, the reader is referred to the web version of this article.)

phosphonates [12]. Selecting appropriate ratio of reactants may be also a key. After many trials of experiments, good quality crystals were obtained with the ratios of reactants as mentioned in the experimental section above. For compound **4**, without NaF, white mixed with yellow powders were obtained. Hence, in the synthesis of compound **4**, NaF which improved the pH value faintly at the same time served as a mineralizer mainly due to the mineralization of fluoride ions [46,47].

3.3. 2D FTIR correlation analysis

According to the analysis of FTIR spectrum above, the bands in the range 400–800 cm^{-1} are ascribed to P–O bending vibrations

(470–620 cm^{-1}) from phosphonate groups and C–H out-of-plane bending vibrations (650–840 cm^{-1}) of aromatic rings from H_3L^1/H_3L^2 ligand. The characteristic bands in the range 900–1200 cm^{-1} are attributed to P–O stretching vibrations from phosphonate groups. The special band around 1700 cm^{-1} is attributed to the absorption of the protonated carboxyl group. The sharp bands in the ranges of 1650–1500 and 1450–1350 cm^{-1} are assigned to the asymmetric and symmetric stretching vibrations of carboxyl groups, respectively [48]. The characteristic bands in the range of 2200–2800 cm^{-1} are ascribed to the stretching vibrations of (P–)–O–H···O hydrogen bonds via the protonated phosphonate groups. In order to clarify the structural changes of functional groups from H_3L^1 and H_3L^2 ligands in the compounds more efficiently, 2D FTIR correlation analysis is applied in the regions as mentioned above. Herein we analyze the selected 2D FTIR correlation spectra of the compounds for comparison. Figs. 13–16 depict the synchronous 2D FTIR correlation spectra of the compounds with thermal and magnetic perturbation.

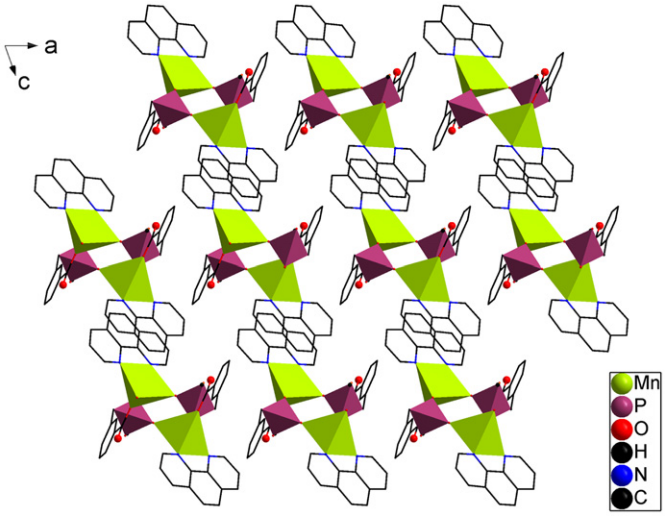

Fig. 12. A view of crystal packing diagram of compound **4** on *ac* plane; the H atoms attached to C atoms are omitted for clarity; polyhedron color codes: Mn (yellow-green polyhedron), P (purple polyhedron). (For interpretation of the references to color in this figure legend, the reader is referred to the web version of this article.)

As shown in Fig. 13(a), there is a strong autopeak along the diagonal line at 540 cm^{-1}, which demonstrates that P–O bending vibrations are sensitive to thermal perturbation. A weak autopeak along the diagonal line is also detected at 760 cm^{-1}, which indicates C–H out-of-plane bending vibrations of aromatic rings from H_3L^1 ligand are faintly sensitive to thermal perturbation. But in Fig. 13(b), a strong autopeak along the diagonal line is detected at 660 cm^{-1} and only two autopeak packages appear at 415 and 595 cm^{-1} with magnetic perturbation. In Fig. 14(a), there are three strong autopeaks along the diagonal line at 930, 945 and 1065 cm^{-1}, which indicate P–O stretching vibrations are sensitive to thermal perturbation, while in Fig. 14(b), only two autopeak packages along the diagonal line around 1000 and 1130 cm^{-1} can be detected with magnetic perturbation. According to the analysis above, it can be concluded that that P–O vibrations from phosphonate groups are sensitive to thermal perturbation while C–H out-of-plane bending vibrations of aromatic rings from H_3L^1 ligand are sensitive to magnetic perturbation may be due to the anti-magnetic ring current generated by π-electronic system of aromatic rings in magnetic field.

As shown in Fig. 15(a), there are two strong autopeaks along the diagonal line at 1400 and 1555 cm^{-1}, which demonstrate that the symmetric and asymmetric stretching vibrations of carboxyl

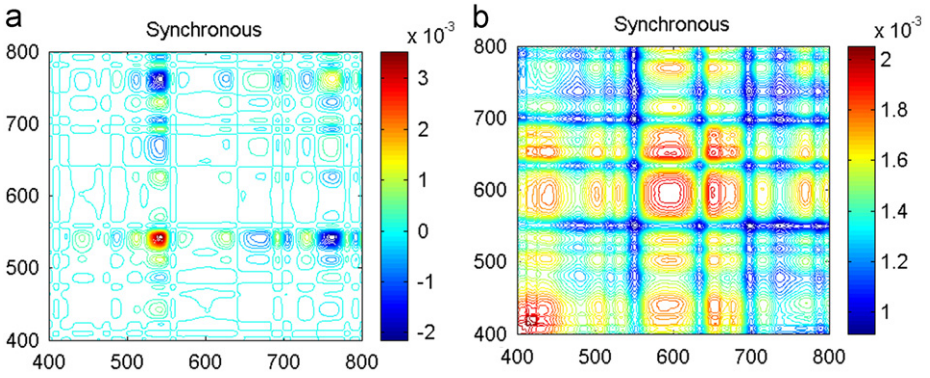

Fig. 13. The Synchronous 2D FTIR correlation spectra of **1** in the range 400–800 cm^{-1} (a) with thermal perturbation (b) with magnetic perturbation.

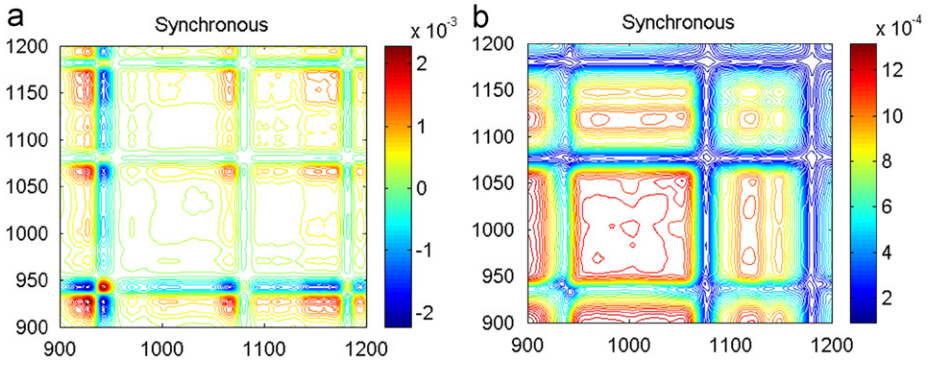

Fig. 14. The Synchronous 2D FTIR correlation spectra of **4** in the range 900–1200 cm^{-1}. (a) with thermal perturbation (b) with magnetic perturbation.

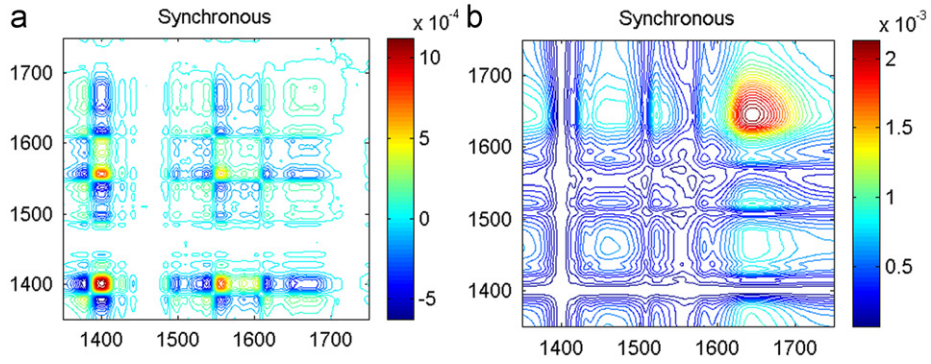

Fig. 15. The Synchronous 2D FTIR correlation spectra in the range 1350–1750 cm^{-1}. (a) **2** with magnetic perturbation (b) **4** with magnetic perturbation.

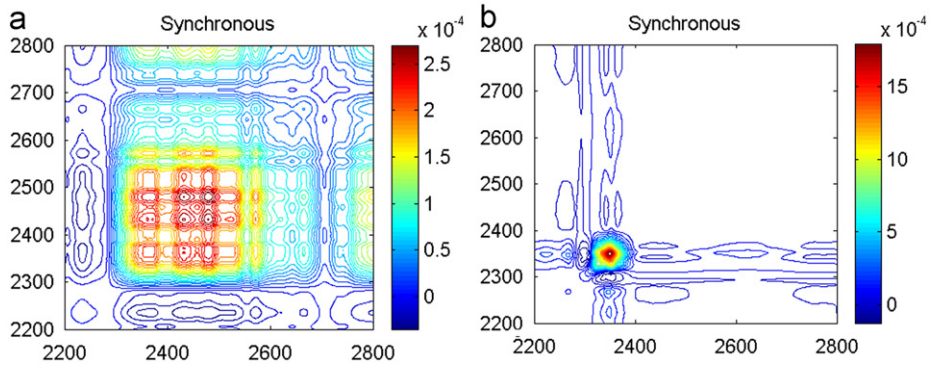

Fig. 16. The Synchronous 2D FTIR correlation spectra in the range 2200–2800 cm^{-1}. (a) **3** with thermal perturbation (b) **4** with thermal perturbation.

groups are sensitive to magnetic perturbation. In Fig. 15(b), there is a strong autopeak along the diagonal line at 1660 cm^{-1} and a weak autopeak along the diagonal line at 1455 cm^{-1} (may be due to the coordination mode of the carboxyl groups) with magnetic perturbation. The difference between the asymmetric and symmetric carboxyl groups stretchings, $\Delta(\Delta=\upsilon_{as}-\upsilon_{s})$, suggests the coordination modes of the carboxyl groups [34,48]. From the analysis of Fig. 15(a) and (b), no absorption of deprotonated carboxylic groups appearing around 1700 cm^{-1} of 1D FTIR spectra could be demonstrated via the 2D FTIR correlation spectra with magnetic perturbation. Moreover, Δ of compound **4** covers a broader range than that of compound **2,** consistent with the coordination modes of the carboxyl groups in both compounds.

As shown in Fig. 16(a), there are three strong autopeaks along the diagonal line at 2365, 2425 and 2455 cm^{-1}, of which the two autopeaks at 2425 and 2455 cm^{-1} could be ascribed to the same kind of stretching vibrations of (P–)–O–H···O hydrogen bonds while in Fig. 16(b), only one strong autopeak along the diagonal line at 2350 cm^{-1}. Comparing the 2D FTIR correlation spectra with thermal perturbation of the two compounds in the range 2200–2800 cm^{-1}, there should be two types of (P–)–O–H···O hydrogen bonds in compound **3** and one type of (P–)–O–H···O hydrogen bond in compound **4**. The results are consistent with the structures of both compounds.

4. Conclusion

In conclusion, four novel divalent transition metal carboxyarylphosphonates were synthesized under hydrothermal conditions with two phosphonocarboxylic acids just of different substitution modes and two divalent transition metal ions, Ni(II) and Mn(II), in the presence of the auxiliary ligands 4,4′-bipy(4,4′-bipyridine) and phen(1,10-phenanthroline). The four compounds exhibit diverse structural chemistry. **1** features 1D linear chains built from Ni(II) ions bridging 4,4′-bipy. In **2**, neighboring Ni_4 cluster units are connected by pairs of H_3L^2 ligands to form 1D double-crankshaft chains, which are interconnected by pairs of 4,4′-bipy into 2D sheets. **3** exhibits 2D supramolecular layers via the $R_2^2(8)$ ringed hydrogen bonding units. **4** has 1D ladderlike chains, in which the 4-membered rings are cross-linked by the organic moieties of the H_3L^2 ligands. There are 1–3 types of intermolecular interactions in the four compounds, namely, O–H···O hydrogen bonding interactions, C–H···π interactions and π–π interactions. The structures of metal carboxyarylphosphonates are also affected by many synthetic conditions, such as pH value, the ratio of reactants, the nature of metal ion, the introduction of auxiliary ligand(s), etc. Moreover, employing the generalized 2D FTIR correlation spectroscopy can probe the subtle structural changes of functional groups from the H_3L^1/H_3L^2 ligand in the compounds with thermal or magnetic perturbation. So it is worthwhile to explore in-depth function of generalized 2D FTIR correlation spectroscopy. Both H_3L^1 and H_3L^2 ligands have remarkable features and further research on this promising type of ligands could take place to prepare novel metal carboxyarylphosphonate compounds of higher dimensional architectures with other metal ions and auxiliary ligands.

Supplementary data

Crystallographic data for the structures reported on this work have been deposited in the Cambridge Crystallographic Data Center with CCDC reference numbers 759551–759554 for **1**–**4**. These data can be obtained free of charge at www.ccdc.cam.ac.uk/conts/retrieving.html or from the Cambridge Crystallographic

Data Center, 12, Union Road, Cambridge CB2 1EZ, UK; fax: (internat.) +441223 336 033; E-mail: deposit@ccdc.cam.ac.uk.

Acknowledgments

We gratefully acknowledge the financial support from the National Nature Science Foundation of China (No. 20873021), the State Key Laboratory of Structure Chemistry, Fujian Institute of Research on the Structure of Matter, Chinese Academy of Sciences, and the Young Talent Programmed of Fujian Province (No. 2006F3072). We thank Prof. Sun Suqin (Tsinghua University, Beijing, China) for providing the 2D FTIR correlation analysis software.

Appendix A. Supplementary materials

Supplementary data associated with this article can be found in the online version at doi:10.1016/j.jssc.2010.04.037.

References

[1] S.F. Tang, J.L. Song, X.L. Li, J.G. Mao, Crystal Growth & Design 6 (2006) 2322–2326.
[2] C. Lei, J.G. Mao, Y.Q. Sun, H.Y. Zeng, A. Clearfield, Inorganic Chemistry 42 (2003) 6157–6159.
[3] P. Yin, S. Gao, L.M. Zheng, X.Q. Xin, Chemistry of Materials 15 (2003) 3233–3236.
[4] L.M. Zheng, S. Gao, P. Yin, X.Q. Xin, Inorganic Chemistry 43 (2004) 2151–2156.
[5] D.Y. Kong, Y. Li, O.Y. Xiang, A.V. Prosvirin, H.H. Zhao, J.H. Ross, K.R. Dunbar, A. Clearfield, Chemistry of Materials 16 (2004) 3020–3031.
[6] D.M. Poojary, B.L. Zhang, P. Bellinghausen, A. Clearfield, Inorganic Chemistry 35 (1996) 5254–5263.
[7] J.G. Mao, Z.K. Wang, A. Clearfield, Inorganic Chemistry 41 (2002) 3713–3720.
[8] S.Z. Hou, D.K. Cao, Y.Z. Li, L.M. Zheng, Inorganic Chemistry (2008) 10211–10213.
[9] J.L. Song, J.G. Mao, Chemistry—a European Journal 11 (2005) 1417–1424.
[10] S. Bauer, N. Stock, Journal of Solid State Chemistry 180 (2007) 3111–3120.
[11] X.M. Gan, B.M. Rapko, J. Fox, I. Binyamin, S. Pailloux, E.N. Duesler, R.T. Paine, Inorganic Chemistry 45 (2006) 3741–3745.
[12] B.P. Yang, A.V. Prosvirin, H.H. Zhao, J.G. Mao, Journal of Solid State Chemistry 179 (2006) 175–185.
[13] H.H. Song, L.M. Zheng, G.S. Zhu, Z. Shi, S.H. Feng, S. Gao, Z. Hu, X.Q. Xin, Journal of Solid State Chemistry 164 (2002) 367–373.
[14] H.H. Song, L.M. Zheng, Z.M. Wang, C.H. Yan, X.Q. Xin, Inorganic Chemistry 40 (2001) 5024–5029.
[15] D.K. Cao, Y.Z. Li, Y. Song, L.M. Zheng, Inorganic Chemistry 44 (2005) 3599–3604.
[16] A. Clearfield, C.V.K. Sharma, B.P. Zhang, Chemistry of Materials 13 (2001) 3099–3112.
[17] S. Bauer, T. Bein, N. Stock, Inorganic Chemistry 44 (2005) 5882–5889.
[18] D.K. Cao, S.Z. Hou, Y.Z. Li, L.M. Zheng, Crystal Growth & Design 9 (2009) 4445–4449.
[19] J.G. Mao, A. Clearfield, Inorganic Chemistry 41 (2002) 2319–2324.
[20] S.O.H. Gutschke, D.J. Price, A.K. Powell, P.T. Wood, Angewandte Chemie—International Edition 38 (1999) 1088–1090.
[21] R.B. Fu, S.C. Xiang, H.S. Zhang, J.J. Zhang, X.T. Wu, Crystal Growth & Design 5 (2005) 1795–1799.
[22] A. Anillo, A. Altomare, A.G.G. Moliterni, E.M. Bauer, C. Bellitto, M. Colapietro, G. Portalone, G. Righini, Journal of Solid State Chemistry 178 (2005) 306–313.
[23] S. Drumel, P. Janvier, P. Barboux, M. Bujolidoeuff, B. Bujoli, Inorganic Chemistry 34 (1995) 148–156.
[24] N. Stock, T. Bein, Journal of Materials Chemistry 15 (2005) 1384–1391.
[25] N. Stock, T. Bein, Angewandte Chemie—International Edition 43 (2004) 749–752.
[26] Z. Chen, Y. Zhou, L. Weng, C. Yuan, D. Zhao, Chemistry—an Asian Journal 2 (2007) 1549–1554.
[27] Z.X. Chen, Y.M. Zhou, L.H. Weng, D.Y. Zhao, Crystal Growth & Design 8 (2008) 4045–4053.
[28] X.C. Chai, H.H. Zhang, S.A. Zhang, Y.N. Cao, Y.P. Chen, Journal of Solid State Chemistry 182 (2009) 1889–1898.
[29] I. Noda, Applied Spectroscopy 47 (1993) 1329–1336.
[30] I. Noda, Applied Spectroscopy 54 (2000) 994–999.
[31] I. Noda, A.E. Dowrey, C. Marcott, G.M. Story, Y. Ozaki, Applied Spectroscopy 54 (2000) 236A–248A.
[32] Y.N. Cao, H.H. Zhang, C.C. Huang, Q.Y. Yang, Y.P. Chen, R.Q. Sun, F.L. Zhang, W.J. Guo, Journal of Solid State Chemistry 178 (2005) 3563–3570.
[33] Y.P. Chen, H.H. Zhang, X.Z. Wang, C.C. Huang, Y.N. Cao, R.Q. Sun, Journal of Solid State Chemistry 179 (2006) 1674–1680.
[34] S. Zhang, Y.N. Cao, H.H. Zhang, X.C. Chai, Y.P. Chen, Journal of Solid State Chemistry 181 (2008) 399–405.
[35] N.A. Caplan, C.I. Pogson, D.J. Haynes, G.M. Blackburn, Journal of the Chemical Society Perkin Transactions 1 (2000) 421.
[36] G.M. Sheldrick, SHELXL-97, Program for X-ray Crystal Structure Refinement University of Gottingen, Gottingen, Germany, 1997.
[37] G.M. Sheldrick, SHELXS-97, Program for X-ray Crystal Structure Solution University of Gottingen, Gottingen, Germany, 1997.
[38] Y.C. Jiang, Y.C. Lai, S.L. Wang, K.H. Lii, Inorganic Chemistry 40 (2001) 5320–5321.
[39] J. Bernstein, R.E. Davis, L. Shimoni, N.L. Chang, Angewandte Chemie—International Edition 34 (1995) 1555–1573.
[40] Z. Shi, S.H. Feng, S. Gao, L.R. Zhang, G.Y. Yang, J. Hua, Angewandte Chemie—International Edition 39 (2000) 2325–2327.
[41] N. Guillou, Q.M. Gao, M. Nogues, A.K. Cheetham, G. Ferey, Solid State Sciences 4 (2002) 1179–1185.
[42] T. Kurata, A. Uehara, Y. Hayashi, K. Isobe, Inorganic Chemistry 44 (2005) 2524–2530.
[43] M. Mikuriya, K. Tanaka, N. Inoue, D. Yoshioka, J.W. Lim, Chemistry Letters 32 (2003) 126–127.
[44] Z.Y. Du, A.V. Prosvirin, J.G. Mao, Inorganic Chemistry 46 (2007) 9884–9894.
[45] M. Wang, C.B. Ma, D.Q. Yuan, H.S. Wang, C.N. Chen, Q.T. Liu, Inorganic Chemistry 47 (2008) 5580–5590.
[46] J. Kratochvil, M. Necas, V. Petricek, J. Pinkas, Inorganic Chemistry 45 (2006) 6562–6564.
[47] T. Mahenthirarajah, Y. Li, P. Lightfoot, Inorganic Chemistry 47 (2008) 9097–9102.
[48] K. Nakamoto, Infrared and Raman Spectra of Inorganic and Coordination Compounds, Wiley Interscience, New York, 1986.